Ultrafast Dynamics of Single Crystal and Polycrystalline VO_2

Meaghan Daly

Department of Physics, University of Colorado at Boulder
Defended April 2, 2015

Thesis Advisor:
Markus Raschke - Physics

Thesis Committee:
Markus Raschke - Physics
John Cumalat - Physics
Mark Borden - Mechanical Engineering

ABSTRACT

In recent decades, interest has rapidly developed in the group of materials known as strongly correlated electron systems. These systems exhibit numerous startling behaviors ranging from high temperature superconductivity to the topic of this thesis: metal-insulator transitions, specifically in the material vanadium dioxide (VO_2). Unfortunately, due to wide variations within and between samples, it has been difficult to determine the underlying cause of such a phenomenon. In an effort to establish more consistent discrepancies between different growth methods, I have studied two samples of VO_2: a single crystal and a polycrystalline thin film. The differences observed in the responses of each provide validation to further research in this area, if not a fully conclusive result.

KEY TERMS

Strongly Correlated Electron Material: A system in which electrons cannot be considered independent of the quantum structure in which they exist.

Metal-Insulator Transition: A transformation of a material from a metallic (conducting) state to an insulating (non-conducting) state.

Band Structure: A mathematical description of the allowed and disallowed energy states for an electron within a material.

Pump-Probe: A method of observing ultrafast processes within a material by varying the interference between two beams of light (a pump and a probe).

TABLE OF CONTENTS

1. INTRODUCTION

As our knowledge of the quantum workings of atoms and molecules continues to grow, we become able to explore previously incomprehensible phenomena. Recently, there has been a peak in interest in a group of materials known as strongly correlated electron systems which exhibit seemingly inexplicable behavior, such as abrupt transitions from an insulating to a metallic state. These characteristics cannot be explained effectively under the assumption of noninteracting electrons. Thus, the models which describe these materials must account for the interaction between the electrons they contain and the full structure of the quantum system in which they exist.

Vanadium dioxide (VO_2) undergoes one of the most well-known and widely studied metal-insulator transitions. VO_2 has been observed as an insulator in the low temperature (low-T) phase, and yet, as a conductor in the high temperature (high-T) phase. Though there has been a great deal of interest in this behavior, the mechanism of the transition is still under considerable debate.

There are currently two prominent theories for the development of the high-T phase of the material: Peierls structural distortion and Mott-Hubbard electronic correlation [1,2]. Peierls distortion deals with the movement of the physical structure in the crystal. A change in the structure of the nuclei could cause the disappearance of a band gap (an area of no allowed electronic states) and lead to better conductivity behavior [3,4]. Mott-Hubbard electronic correlations, on the other hand, deal with the interactions between electrons. Due to the quantum structure of VO_2, electrons interact much more than in a typical material. These interactions result in the organization of charge carriers, which may decrease the size of the band gap and

cause charge carriers to move more freely [5,6]. Thermal and optical excitation of the samples induces at least one of these effects, which is what (most likely) drives the transition. While most agree that both effects are present, the true debate is over the importance of each [1,2].

One of the primary reasons that this debate has not been settled is due to disorder in the samples being tested. The largest discrepancy comes from the differences in polycrystalline and single crystal samples. The observed variations could indicate that the motivation of the transition depends more heavily upon the growth of the crystal than previously thought [7]. In order to understand the intrinsic behavior of the transition itself, it is important that we observe differences between samples, which may indicate a previously unseen correlation.

In order to further this work, I have performed ultrafast optical pump-probe spectroscopy on two VO_2 samples: a thin film sample and microcrystal sample, under a variety of conditions. These conditions include different power levels of the optical excitation and temperature dependence of the thermal excitation.

As strongly correlated electron materials are not yet widely understood, the practical applications of this investigation are limited. In the long term, increased understanding of materials such as vanadium dioxide could lead to improvements in electronic systems. This may consist of components such as ultrafast transistors, which could greatly improve efficiency.

The results of my specific research serve to increase the knowledge base surrounding metal-insulator transitions. By comparing the signal responses of the polycrystalline and thin-film samples, we may uncover differences in the driving mechanism behind the transition, i.e. the influence of Peierls distortion versus that of the Mott-Hubbard correlation.

For the sake of clarification, this thesis will begin with a section dedicated to the theory behind the behavior observed in vanadium dioxide. Though the details of the interactions within this material are still unknown, it is possible to return to a basic understanding of solid state physics in order to describe what could be happening. In light of this, the following chapter will consist mostly of theoretical discussion and derivation in the hopes of establishing a basis to draw from.

2. BACKGROUND

2.1. Strongly Correlated Electron Materials

The samples I have studied throughout my research fall under the category of strongly correlated electron materials. These systems cannot yet be thoroughly explained by our current understanding of solid state physics due to the fact that the electrons within cannot be considered independent of the quantum structure in which they exist. These materials are typically elements with an open *d* or *f* band, in which the states the electrons may occupy are very narrow. Due to this crowded occupation, the electrons begin to interact with each other coulombically, rather than behaving as though the other electrons did not exist [8,9]. This interaction causes a correlation between the electrons, which significantly modifies the Hamiltonian of the system. This modification will be discussed further in a later section. However, this new interaction can lead to many different phenomena, such as high-temperature superconductors or, the topic of interest in this paper, metal-insulator transitions [10].

2.2. Band Structure

In order to understand the potential forces acting in strongly correlated electron materials, it is necessary to first understand the band structure associated with the systems we are concerned with. Band structure refers to the allowed states the electrons in a material may occupy, deriving from the restrictions placed upon these fermions by the Pauli exclusion principle, which states that no more than one fermion can occupy a specific state at any time.

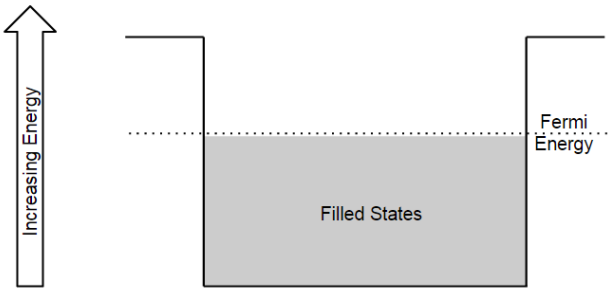

Figure 1 A depiction of the one-dimensional potential well.

The simplest way of thinking about this is in terms of a quantum mechanical approximation. The atom is viewed as a large potential well with its atoms effectively filling up the well to a certain level, as shown in Fig. 1. “Filling up” in this case refers to the filling of electron shell states in accordance with the Pauli exclusion principle mentioned previously. Once these electrons fill up the well as far as they can, it is possible to solve the associated Schrodinger equation for the allowed energies as a function of momentum. The result is as follows:

$$E = \frac{\hbar^2 k^2}{2m}$$

where k is the momentum and m is the mass of the electron.

It is evident from this solution that the energy should go quadratically as a function of momentum. Using the boundary conditions, the solution for k becomes:

$$k = \frac{2\pi}{L}$$

with L as the length of the bottom of the potential well. This solution has approximated the bottom of the potential well as completely flat. This, however, is not the case. The bottom of the well would instead be some function due to the ionic interactions of the electrons with other

nuclei. In fact, the function would actually be periodic with a characteristic length a, as shown in Fig. 2.

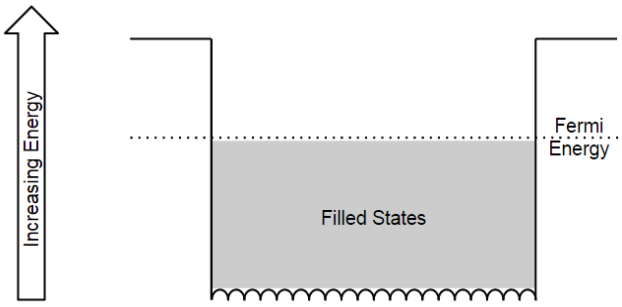

Figure 2 Potential well with periodic base correction.

Furthermore, as the potential well is a periodic function, there should be some finite number of repetitions, n, of the function over the length of the well. This number can be written in terms of the characteristic length, a, and the total length of the well, L:

$$n = \frac{L}{a}$$

Using this, the initial approximation can be modified. Instead of having a single straight line as the bottom of the potential well, it can be rewritten as a piecewise function of n-many straight lines. These piecewise functions should all be the same as the potential is approximated as the same across. This leads to n-many k's. Using this, the equation for k becomes:

$$k = \frac{2\pi}{L} n$$

Using the equation relating n to L and a, this becomes:

$$k = \frac{2\pi}{a}$$

As n is a finite number, k should also be some finite number. Therefore, any k outside of a range with total length $2\pi/a$ is redundant. We choose this range to be centered about k = 0,

which gives possible k values of -π/a to π/a [11]. This principle gives a different representation of the energy versus momentum graph shown in Fig. 3(a). All of the ranges outside of -π/a to π/a can now be folded back upon themselves, as their ranges are just multiples of the original. This results in the crisscrossing pattern shown in Fig. 3(b).

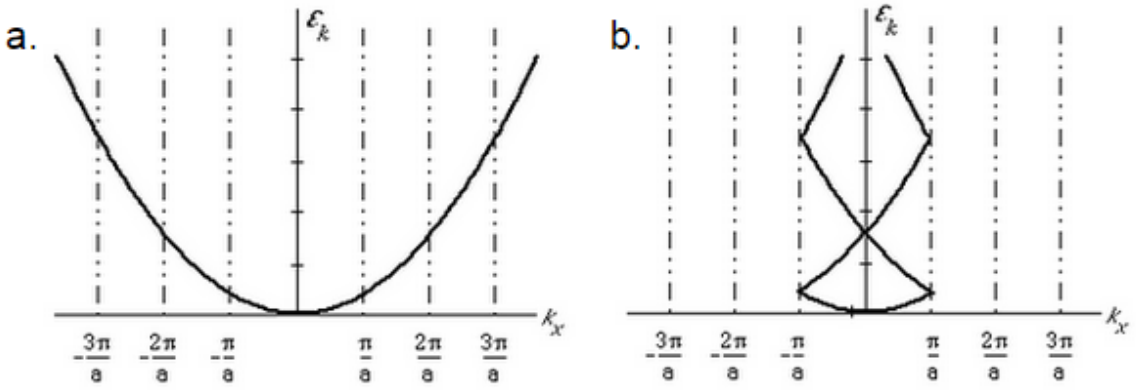

Figure 3 (a) "Free-Electron" Model. This represents the allowed states of electrons in a material. Note that this suggests that electrons could occupy any energy under the correct conditions. (b) Reduced Zone Scheme. This graph, as opposed to the free-electron model, shows that only a finite number of momentum vectors are required to describe the entire band structure of a material. [12]

There is one last correction to be made to this picture. Due to the Pauli exclusion principle, the points where the lines cross on Fig. 3(b) are not allowed as they would imply two electrons occupying the same state. Using degeneracy theory, it is possible to remove these intersections leaving, in place of two states with the same energy, one state with energy slightly lower than the original and one state with energy slightly higher. This separation is then referred to as a bandgap [11]. This correction leads to the actual representation, as shown in Fig. 4, known as the reduced zone scheme .

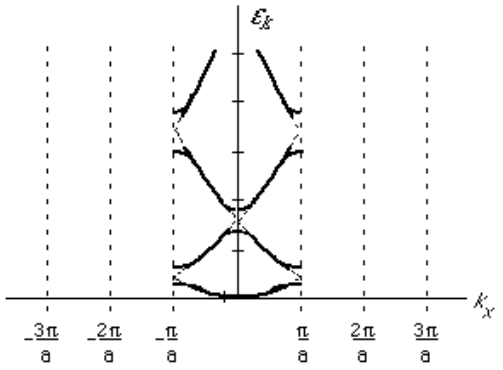

Figure 4 Reduced zone scheme with degeneracy corrections. In this representation, as opposed to the original free-electron model, note that it is no longer possible for an electron to exist at every energy. These regions of forbidden states are crucial to understanding the range of behaviors we observe in materials, i.e. the distinction between metals, semiconductors, and insulators. [12]

By looking at the location of the Fermi energy, the ground state energy of an atom, in diagrams such as these, we can describe the differences between metals, semiconductors, and insulators. In order to be a metal, a material must be able to conduct electricity, i.e. the electrons in the material must be able to reach a state above the Fermi energy such that they are in the conduction band and are free to move away from the nucleus. This implies that, in a metal, the Fermi energy will occur in a region of allowed states. In a semiconductor, the Fermi energy occurs at the boundary of a region of allowed states where the next region of allowed states is relatively close. In this state, it would be easy to excite the electrons over the forbidden states and into the conduction band. A similar scenario is true for insulators: the Fermi energy occurs at the boundary of a region of allowed states. However, in this case, the next region of allowed states is relatively far away, such that it would be very difficult to excite electrons into the conduction band [13]. A depiction of the Fermi energy location in these materials is shown in Fig. 5.

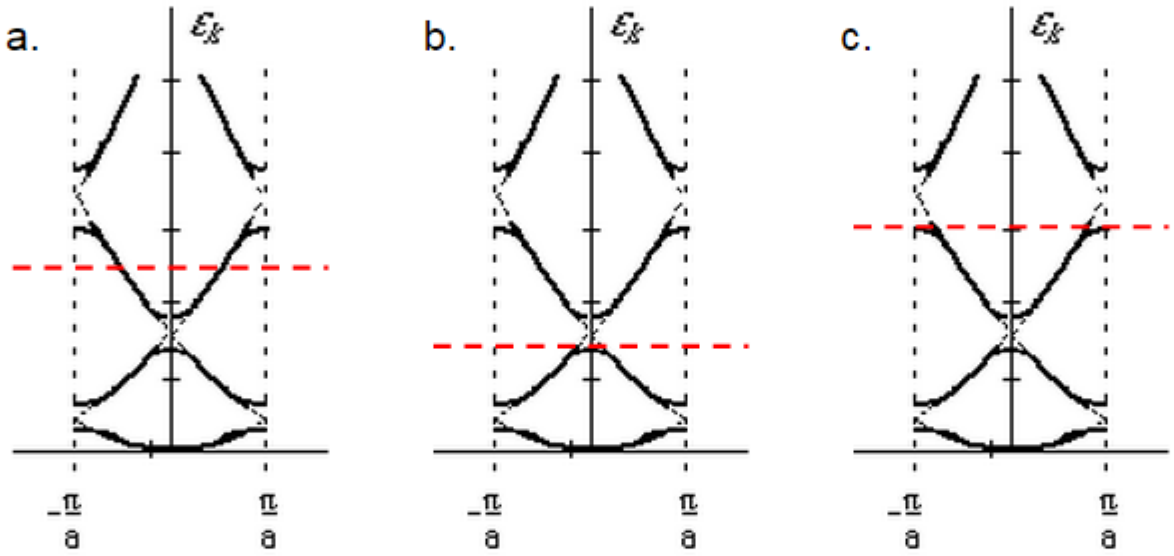

Figure 5 Fermi energy level location in a (a) metal, (b) semiconductor, and (c) insulator. Note that in both the semiconductor and the insulator the Fermi level exists at the limit of a region of allowed states. This is due to the fact that, at a temperature of 0K, electrons should fill up the available states of an atom to exactly the Fermi energy level, per its definition. Therefore, the Fermi energy must exist at a location that the electrons can fill up to it. [12]

The interactions that take place in a metal-insulator transition within a strongly correlated electron material are results of changes in the band structure of the material which results in a change in the location of the allowed states relative to the Fermi energy.

2.3. Peierls Distortion

The first of these changes is Peierls distortion. This effect is a physical distortion of the nuclei in the molecule. For clarity's sake, it is important to realize that this is not an effect of electron correlation and, as such, does not apply to strongly correlated electron materials in general. In the case of VO_2, however, there is a change in the lattice structure through the transition [4]. This may suggest that, though it is not what qualifies vanadium dioxide as a strongly correlated electron material, it is a large contributing factor to the response we observe.

The result of the physical distortion is a change in the structure of the potential the electrons exist in. The bottom of the well is still periodic but now, instead of the characteristic length being just "a", it is some different number. This changes the range of k, which means that instead of folding back the original parabola at π/a, it is folded back at some other point. This changes the locations where the lines cross, i.e. the locations of the bandgaps. The distortion can, therefore, open a bandgap in a new location effectively disallowing the electrons to pass above the Fermi level and changing a metal into an insulator or visa versa [11].

2.4. Mott-Hubbard Correlation

The second possible change is Mott-Hubbard correlation. This effect is not as physically based as the Peierls distortion. Instead, it deals with the electrons positions relative to each other. Typically, in any material, it is assumed that the electrons are isolated. On the contrary, in a material such as vanadium dioxide, the electrons cannot be considered independent of their neighbors. They are, instead, able to "see" each other.

The typical assumption of isolation is valid in most cases due to the extremely small magnitude of the Coulomb repulsion between electrons. In strongly correlated electrons materials, this force is too large to be ignored. In some cases, it is even large enough to create a meaningful distortion in the potential of the crystalline structure and open up bandgaps where the electrons simply cannot get any closer to each other. The Hamiltonian for a Mott-Hubbard insulator is:

$$H = -\sum_{<i,j>,\sigma} t_{ij}(c_{i\sigma}^{\dagger}c_{j\sigma} + c_{j\sigma}^{\dagger}c_{i\sigma}) + U\sum_{i} n_{i\uparrow}n_{i\downarrow}$$

The first term gives electron "hopping",transfer between two adjacent lattice states. The second term is the main concern here. It represents the onsite repulsion between two electrons. U is the energy from the Coulomb interaction of the electrons. If we take this value divided by the magnitude of t_{ij}, the overlap bonding integral (a measure of the overlap between adjacent electron orbitals), we can assess the extremes of this equation. In the limit where U/t_{ij} is much less than 1, the second term disappears and the Hamiltonian becomes that of a free Fermi gas, the "free electron model". On the contrary, in the limit where U/t_{ij} is much greater than 1, the first term becomes negligible and there is a finite coupling between lattice sites, the "tight binding model" [14]. A representation of the allowed states for electrons as we vary this ratio is shown in Fig. 5.

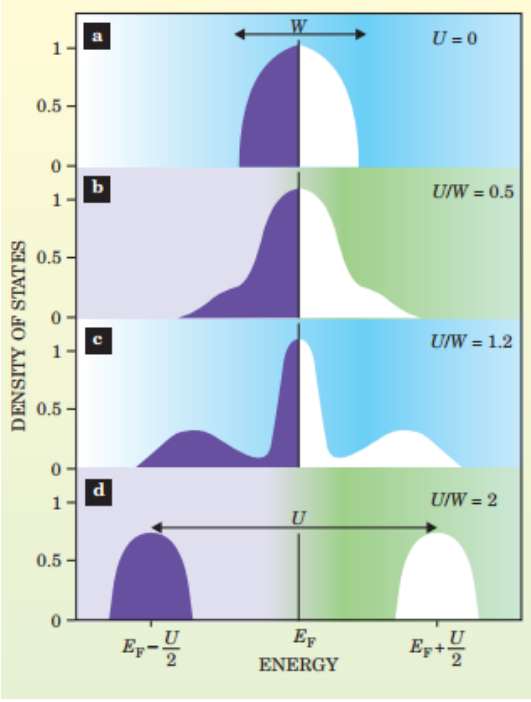

Figure 5 The locations of allowed electron states for various values of U/W. In this figure, U is still the energy from the Coulomb interaction and W is the overlap bonding integral (mentioned above as t_{ij}). Notice that at $U = 0$, the allowed states encompass the Fermi energy, allowing excitation into the conduction band (as in a metal). As U/W becomes greater, however, the allowed states split, creating a bandgap over the Fermi energy and trapping the electrons in the valence band. [8]

2.5. Vanadium Dioxide

It has been hypothesized that both of these effects occur in vanadium dioxide. The main argument is over the prevalence of each in the driving force of the metal-insulator transition. At low temperatures, i.e. low energy, VO_2 is an insulator, suggesting that it is in this state that the crystalline structure is distorted in a way that both Peierls distortion and Mott-Hubbard correlation take effect. At high temperatures, however, VO_2 is a metal with a higher crystalline symmetry, which would imply a lack of the Peierls distortion.

Unfortunately, the exact contributions of each of these phenomena within the metal-insulator transition of VO_2 are still unknown. Though it is certain that there is a change in the lattice structure of the material [4], it is unclear whether or not this is the only factor contributing to the appearance of two states [1,2]. There is evidence that the electronic behavior is the predominant cause, but this is not yet conclusive [5,6].

The fault of this ambiguity partially falls upon the variety of samples being tested. It has been demonstrated that the response of single crystal VO_2 alone is inhomogeneous [7]. The thermally induced excitation produces irregularities in the metallic state, as shown in Fig. 6.

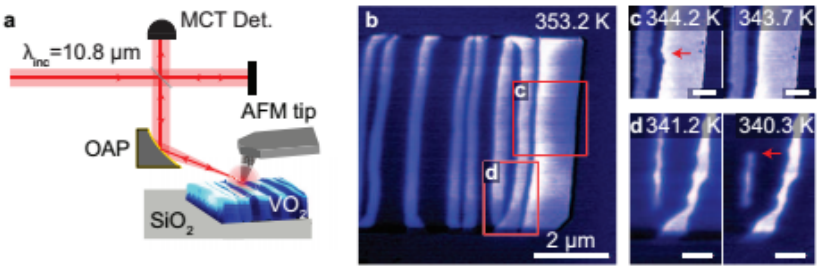

Figure 6 (a) Schematic of Drude response scattering scanning near-field optical microscopy (s-SNOM), the method by which these scans were taken. (b) An image of the irregularities in a microcrystal through heating. The light areas are metallic while the dark area are insulating. (c) and (d) The effect of cooling on the microcrystal. The metallic areas gradually shrink as temperature decreases. The locations of these irregularities changes between cooling cycles. The scale bars in panels of c, d are 500 nm and 200 nm, respectively [7].

In addition to this, the timescale of the transition can also range from 40 to 200 femtoseconds across different samples. This large variety would suggest that the transition is highly dependent on defects in the sample or the method by which it was created [7]. This is further elaborated upon in Fig. 7.

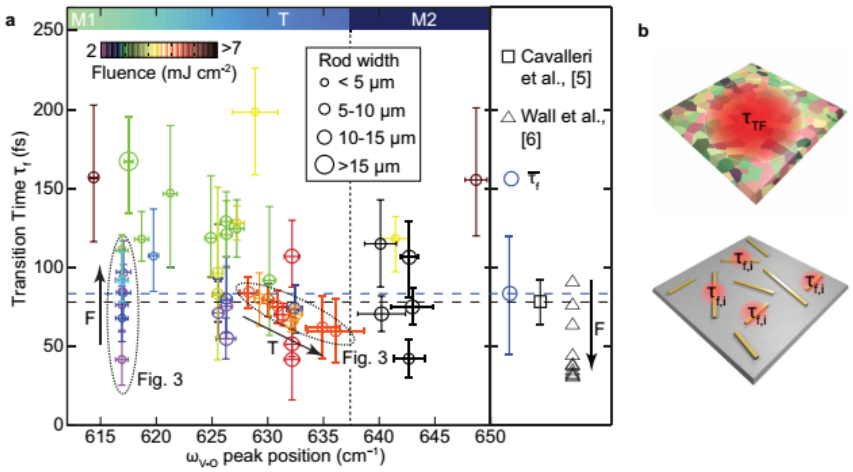

Figure 7 (a) Photoinduced transition time, τ_f , VS initial insulating phase (indicated at top). Symbol size indicates microcrystal width (less than 5 μm to more than 15 μm). Symbol color indicates pump fluence. Dashed ovals indicate data sets. (b) Polycrystalline sample (thin film - top, τ_{TF}) vs single crystal (bottom $\tau_{f,i}$). [7]

In addition to this, within VO_2, there are three distinct insulating phases: monoclinic 1 (M1), monoclinic 2 (M2), and triclinic (T) and one rutile metallic phase (R). M2 is characterized by a dimerization of vanadium atoms along the cR axis. M1 is characterized by the rotation of this dimer. T is a continuous distortion of the M1 phase. These are depicted in Fig. 8. M1 is the most stable phase for VO_2 at room temperature [15].

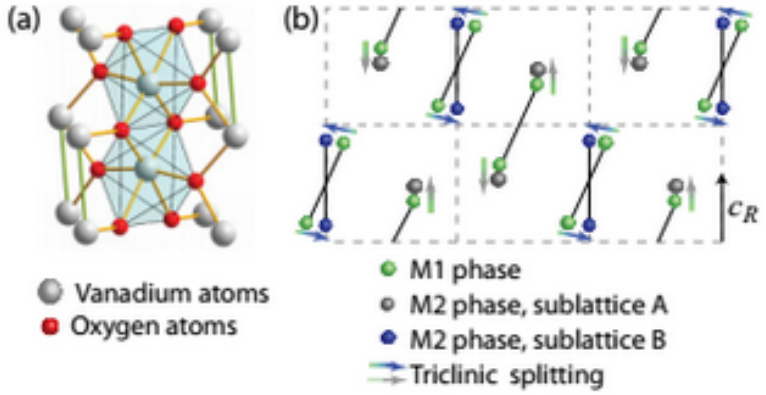

Figure 8 (a) VO_2 structure showing the oxygen and vanadium surrounding the vanadium sublattices. (b) Positions of the vanadium atoms in the M1 and M2 phases. Note that T is somewhere between these two states [15].

These phases are a result of increasing tensile strain on the crystalline structure of the material. Differences in strain actually result in a change in the response of the sample. It has been demonstrated that increasing tensile strain in a sample of VO_2 causes a movement in the corresponding Raman shift (a method of spectroscopy used to determine chemical compositions) [15]. The results of this experiment are shown in Fig. 9, below.

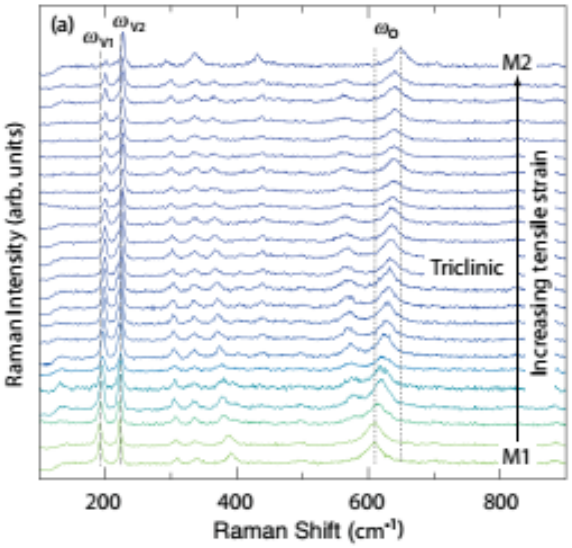

Figure 9 Raman spectra of a VO_2 microcrystal subjected to increasing tensile strain at room temperature. [15]

3. METHODS

3.1. Pump-Probe Spectroscopy

One of the difficulties of this experiment is that the transition in vanadium dioxide occurs on the order of femtoseconds: much too fast to observe with conventional methods. Because of this, I had to look at the transition in a different way.

Though we mostly care about the change in conductivity between the metallic and insulating states, there is a secondary quality which is crucial to observation. Between the metallic and insulating states there is a rather large change in reflectivity. With sufficiently high light intensity, we may photo-induce this transition on sub-ps timescales and, using short enough pulses, we can actually achieve time resolution by measuring the intensity of the light reflected.

Pump-probe spectroscopy does exactly this. The method involves applying two different beams to one sample. These beams can either come from the same source, i.e. two beams of the same wavelength, or from two distinct sources. The first beam, the pump, is the stronger of the two. This beam is used to initially excite the sample. The second beam, the probe, is much weaker than the pump. This beam is designed to be so weak that it will not transfer the energy required for the sample to undergo a transition. In this way, the probe is simply that, a way to measure the reflectivity of the sample without causing a change in its structure.

In order for this to work, the beams must both be pulsed, meaning that, instead of a continuous bombardment of the sample, the laser only sends in light for approximately 50 femtoseconds at a time. This ensures that both beams (primarily the pump) are only able to interact with the sample for a fixed duration such that, rather than seeing only a continuous excitation of the molecules, we can observe the dynamics of the transition.

We achieve the visualization of the transition by varying the relative positions of the pump and the probe in time. We manage this by changing the path length, specifically of the pump. A longer path length takes the light more time to travel which results in the pump hitting after the probe. In this case, the probe would be measuring an unexcited signal and would therefore have the higher reflectivity of the insulating state. On the contrary, if the path length was shorter for the pump, it would hit the sample before the probe meaning that the probe would be measuring the excited metallic state of the sample - a lower reflectivity.

For the sake of clarification, the change in reflectivity in vanadium dioxide is rather counterintuitive to what would normally be assumed. The insulating state actually has a much higher reflectivity than the metallic state at 800 nm (the wavelength I have used in my experiments) [16].

The difference in time between the incidence of the pump and the probe is a variable called “time delay”. By plotting the reflectivity (which is proportional to the intensity on the photodetector) against this variable, we are able to look at the timescale on which the transition occurs. The resolution we are able to achieve is equal to the duration of the pulses being emitted from the laser as the smallest interaction the probe can have with the sample is the duration of that pulse. This is on the order of 50fs.

3.2. Pulsed Lasers

However, before any of this can work, we need a laser that produces light in pulses rather than a continuous beam. There are several methods by which this is achieved, but the one I have used in my experiments works on a basis of mode-locking.

The portion of the laser that produces pulses is known as the oscillator. This process begins when the beam from a seed laser (a diode laser which produces 532 nm light) is sent into the oscillator cavity. The light is then focused onto a titanium-doped sapphire (Ti:saph) crystal. This crystal is the gain medium of the oscillator, the source responsible for light amplification by stimulated emission of radiation, i.e. lasing. This is due to a four level system within the Ti:saph. The green photons from the seed laser enter the crystal and excite the atoms from the ground state to a higher state, three energy levels up, creating a population inversion. The excited atoms almost instantaneously (on the order of nanoseconds) drop one level, releasing some amount of heat. A much longer time later, the atom will drop down another energy level. This time, however, instead of releasing heat, the excited atom emits a photon of approximately 800 nm wavelength. The atom then instantaneously (again, on the order of nanoseconds) decays back down to the ground state and the process repeats. This mechanism is illustrated in Fig. 10.

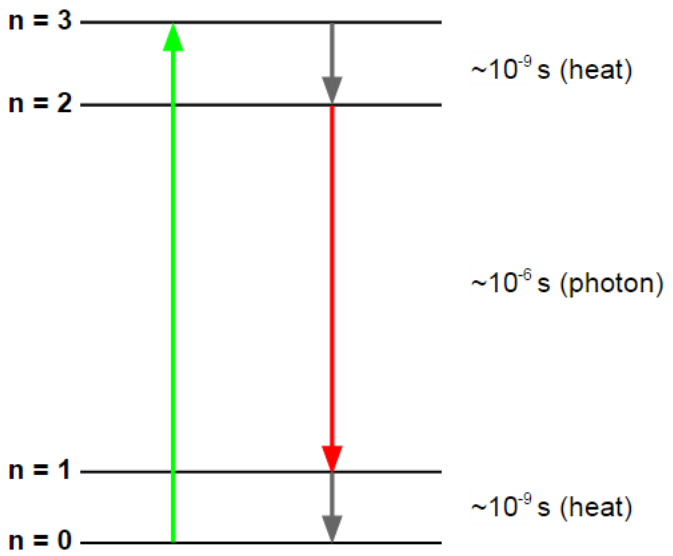

Figure 10 Lasing in a Ti:saph. The seed laser (532 nm) initially excites the atom up to the third energy level. After an immediate drop to the second energy level from heat release, the atom rests in a metastable state. The next drop (from n = 2 to n = 1) results in the emission of a photon of approximately 800 nm wavelength. The atom then decays once more, again releasing heat.

If the second level in this system was always at the same energy, the Ti:saph would only produce one frequency of light: that equal to the energy difference between levels one and two. Yet this is not the case. Instead of a fixed energy difference between these two levels there is a small variation which leads to multiple frequencies of produced light. The range of these frequencies is called the bandwidth of the gain medium. In the case of Ti:saph, it is approximately 128 THz (or 300 nm) wide.

The length of the oscillator cavity limits the frequencies of light that are present. Due to a combination of constructive and destructive interference along the light's path, the only allowed wavelengths are those for which the following relation holds:

$$L = \frac{n}{2}(\lambda)$$

where L is the length of the cavity, n is some integer, and λ is the wavelength. Working with this requirement, within the Ti:saph cavity, there are several hundred frequencies present, all at different phases. At this point, if we were to introduce a small perturbation, then there would be some time during the disturbance at which the frequencies were all phase matched. At all other times, the frequencies would all be destructively interfering to the point of creating nothing but noise in the intensity of light travelling through the cavity. At the point where all the frequencies were phase matched, however, they would constructively interfere, creating a small bump in the signal [17]. This is illustrated in Fig. 11.

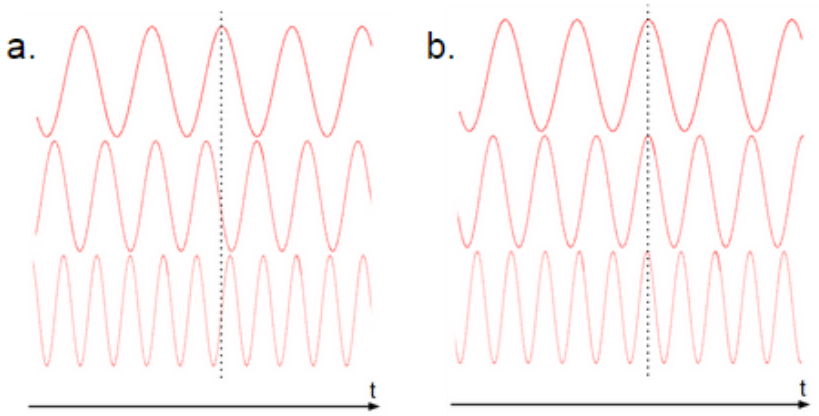

Figure 11 Cavity frequencies in the time domain (a) before perturbation (out of phase) and (b) at some point during perturbation (phase-matched).

As titanium-doped sapphire is a nonlinear gain medium, the point at which the light is focused inside the crystal will change how much gain (increased power) the laser receives. If the light during the perturbation is focused to a point in the crystal where the gain favors higher intensity, the small bump due to phase-matching will have a much higher gain than the noise surrounding it in the time domain. As this bump continues to make trips around the cavity, it will be amplified more and more until it gets to the point where it is such a high intensity that the noise surrounding it is effectively zero. This is the pulse: a high intensity peak in the time domain. A visualization is shown in Fig. 12.

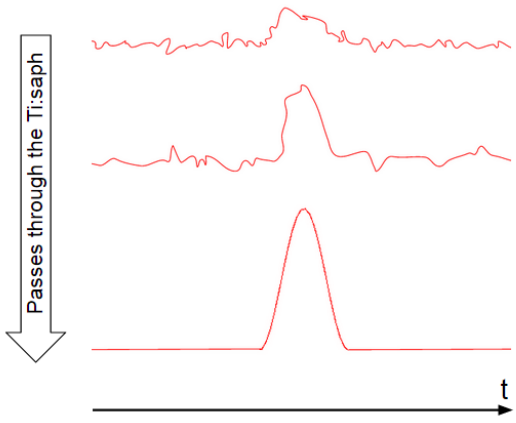

Figure 12 Multiple passes through the gain medium result in an amplification of the phase-matched waves.

The laser produces multiple pulses by bouncing the light off an output coupler, an optic which lets a small portion of the pulse through while reflecting the rest. The time between pulses from the output is the time it takes the single pulse inside the cavity to make one round trip [18].

In order to obtain the time duration of these pulses, we use a method known as Frequency-Resolved Optical Gating (FROG). This method is analogous to that of pump-probe spectroscopy. By interfering two pulses from the same laser in a nonlinear medium (similar to a Ti:saph), we can generate a frequency of light unique to the mixing of the two pulses. By varying the time delay between these pulses, we can obtain a rough estimation of the pulse duration. If we also record the frequency generated over this scan, we can resolve this rough approximation and reconstruct the pulse in order to obtain a much more accurate value [19].

4. IMPLEMENTATION

4.1. Pump-Probe Apparatus

When I began this project, I was fortunate enough to inherit a pre-built pump-probe optical apparatus. As this system had already been calibrated, I began with the assumption that very few drastic changes would need to take place in order to bring it back up to operational status. With the assistance of the graduate student who had been previously working on this project, Brian O'Callahan, I attempted an initial realignment of the system. The apparatus is depicted in Fig. 13.

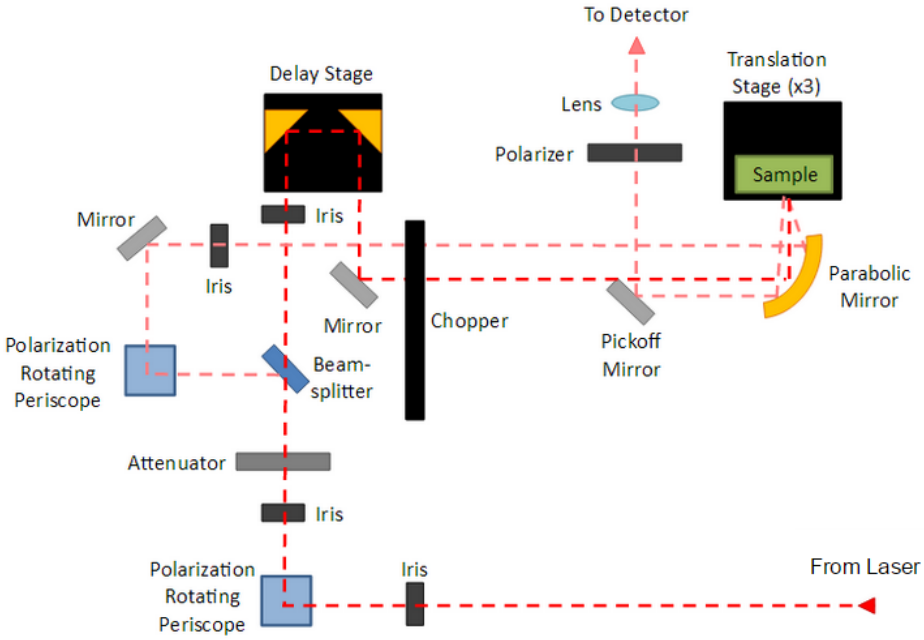

Figure 13 Pump-probe system. We used a Ti:saph laser at 75kHz and adjusted the fluence of the beam via the attenuator. The dark red outlines the pump beam's path while the pink outlines the probe's.

We began by directing a Helium-Neon (HeNe) laser into the system. Using two steering mirrors outside of the pump-probe cavity, we directed the beam through a set of two irises, one outside of the cavity and one inside. We then used the periscope to direct the beam through an

additional two irises inside the cavity. This produced a very rough alignment which we would later be able to fine-tune.

Once roughly aligned, a pellicle was placed in the system to direct the light coming off the sample to a camera connected to a small black and white television. By looking at the television screen, we were able to adjust the direction of the pump and probe beams such that they were overlapped. This visual was also crucial to ensuring that the beams were, in fact, focused on the sample. If they were not, they would appear as lopsided or spread out. In this case, we were able to change the position of the y-translation stage the sample was placed on such that the sample was at the focus of the parabolic mirror and the beams appeared as small circles.

Once the beams were in position, we had to make sure they were hitting VO_2 rather than substrate. This was achieved by blocking the beams and shining a white light source on the sample in their place. This illuminated the surface of the sample which we were then able to move around using the x and z-translation stages (without changing the focus of the beams). The image of the focused beams and a particular VO2 rod are shown in Fig. 14. Note that it was not necessary to find a particular crystal on the polycrystalline sample as the entire surface of the sample is covered in crystals.

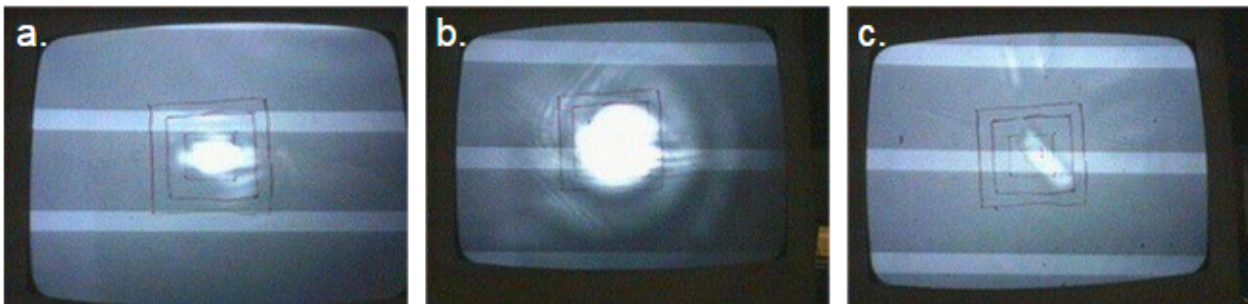

Figure 14 (a) Focused probe beam. (b) Focused pump beam. (c) Rod on the sample.

We were also able to measure fluence, the power per unit area hitting the sample, by using the television screen and laser parameters. The screen is marked with squares of side length 5, 10, and 15 microns. By comparing the pump beam to the squares, we were able to determine the area the pump was affecting. Using the repetition rate (how many pulses are released from the oscillator per second) and the power output of the laser after the attenuator in the system, we could use the following formula to determine fluence:

$$fluence = \frac{(repetition\ rate)(average\ power\ of\ laser\ after\ attenuator)}{(pump\ beam\ spot\ size)}$$

Once the sample was in position, we were able to take a preliminary scan on the rod using the original program created for the system. The results are shown in Fig. 15.

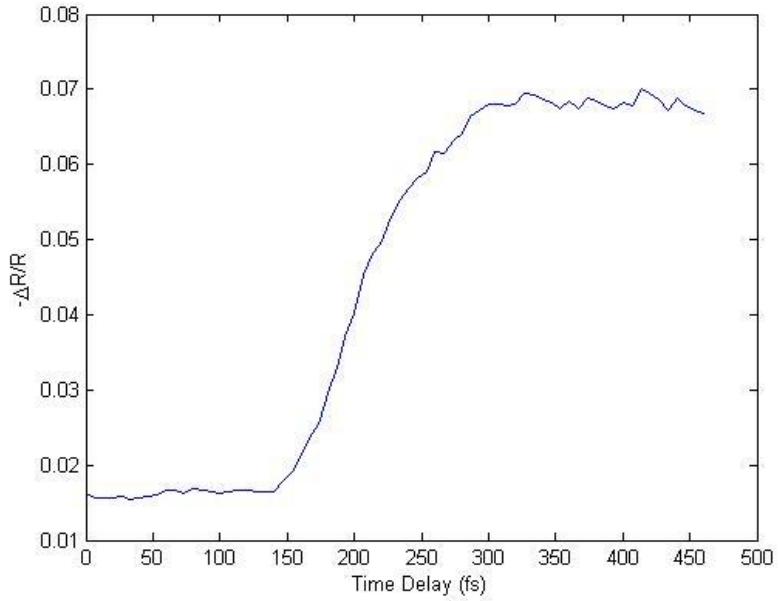

Figure 15 Preliminary scan of VO_2 single crystal sample. At this fluence, we observed the full transition to the metallic state. The lower section of the graph (on the left) is the insulating state while the higher section (on the right) is the metallic state.

It is also important to note that, while it would appear that the metallic state of this material is more reflective than the insulating state, this is not the case. As previously mentioned,

vanadium dioxide, in its metallic state, actually has a much lower reflectivity than the insulating state at 800 nm (the wavelength I will be using). For this reason, the figures presented in this paper have a y-axis proportional to the negative reflectivity. This is meant to allow the figures to make more sense intuitively but it is important to keep this convention in mind.

4.2. Scanning Program

Once the integrity of the system had been verified, I moved on to the actual method of data collection. In order to look at the transition, I needed a program which would be able to plot the intensity being read from the photodetector against the difference in time between the pump and the probe. A program had already been written for the system when I began my work but this program was slow and unreliable. I rewrote the program in LabView in order to remedy these errors.

The program begins by sending the delay stage to a position chosen by the user. Each position on the delay stage corresponds to a certain time delay which was calculated by measuring the lengths of the pump and probe paths with the stage at a known position. By dividing the difference in path lengths by the speed of light, one can obtain the time delay between the two pulses at that position. As the stage is controlled by a piezo, the position relative to the original measured position is very well known. Using this, it was possible to assign each position on the stage to a time delay between the two pulses. This calibration was done during the creation of the original program and transferred to the new program I wrote.

Once the delay stage is in position, the program begins to gather data from the the lock-in amplifier. A lock-in amplifier acts as an intermediary between the photodetector and the

computer. True to its name, it effectively locks on to a certain signal frequency and then measures only the data coming in at that frequency. For the sake of these experiments, the lock-in amplifier was set to the mixing frequency of our pump and probe. This ensures that we are actually measuring a region where both the pump and the probe are interacting with the sample, rather than a region where only the probe is located. It acts as a secondary verification of the system's alignment.

The program gathers data from the lock-in for some amount of time set by the user. It then takes the change in this value over the entire collection time and divides this by the average value over that time. This method gives:

$$\frac{\Delta R}{R} = \frac{(change\ in\ reflectivity)}{(reflectivity)}$$

The benefit to measuring this over just measuring the reflectivity is a dramatic reduction in noise which allows for better fitting and interpretation.

Once this value is calculated, it is plotted against the time delay corresponding to stage position and saved in an array. The data can then be exported from the program as a text file once the scan is complete.

The first priority of my revision was simplification. The program I started with had four separate tabs for different operating modes of the program. Though this had been necessary for previous projects, my experiment only required half of what was available. This surplus of options made it very difficult to navigate the program and even more confusing to troubleshoot it when something went wrong. I began by opening a new program and only copying over the portions of the program that were absolutely necessary for the experiments I wanted to do.

My secondary priority was improving efficiency. The scans we took with the initial program seemed to work well for the first couple data points it collected but it would soon slow down to the point of estimating around 24 hours for the completion of one scan. As I wanted to take quite a few scans and had limited access to the table due to other very sensitive experiments, this was something that had to be fixed.

After going through the program and tracing the path of completed operations, I determined that one potential source was the communication between LabView and the interfacing programs for the delay stage. One of the tabs was designed to run an initialization for the motorized stage which meant that every time the program was stopped, the stage had to be reinitialized. From my experience on other projects that had used similar stages, I knew that this section of the program could be completely removed. Instead of having the program initialize the stage, I could use a separate program that came with the stage's software and would only have to initialize once, regardless of whether or not I had to stop the scan.

Though this did improve communication with the delay stage, the scanning program was still estimating outrageous amounts of time to complete a scan. After additional troubleshooting, I discovered that the problem stemmed from the communication between LabView and the interfacing software for the lock-in amplifier. Though the stage was free to move and would respond without delay to the commands sent from the program, the signal reading required for the program to proceed was taking a very large amount of time to process. This was because the contact between the lock-in and LabView was only established when the program was started for the first time. This same line of contact was then used until the program was stopped completely

and then reopened. In the case of the delay stage, this was not a problem. But for the lock-in, it created a very large backup of old data.

The signal from the lock-in had to be taken as an average over a certain period of time. The program would, therefore, store all the data points taken in that amount of time and then take an average to put into the array. But because contact was only established at the beginning of the program, it kept storing the data from the lock-in, instead of dumping it after each point. I remedied this by reworking the program to establish contact at the beginning of a data point and then sever the connection once the data point was taken. This forced LabView to get rid of all the data it had stored up for the previous data points and greatly improved the speed. Though it would have been ideal to initialize contact with the lock-in software only once, establishing contact only took about a second - a great improvement over the many minutes that resulted from the data backlog.

After testing the new program, I was able to use it to take a fair amount of data. Later in the experiment, I revisited the program to make a few final adjustments. As data collection began, it became clear that it would be valuable to see the progress of the scan in real time. Though it was not possible to have the graph with corrected axes plot the data as the scan advanced (due to limitations within LabView programming), I was able to add a crude chart that would plot the unedited signal as it scanned. I also exported the LabView program to a ".exe" file. This was extremely convenient as the installation of LabView can be lengthy and takes up a fair amount of space on a computer. The new program runs as an executable file which allows it to be easily run on any computer without further hassle. The final program is shown in Fig 16.

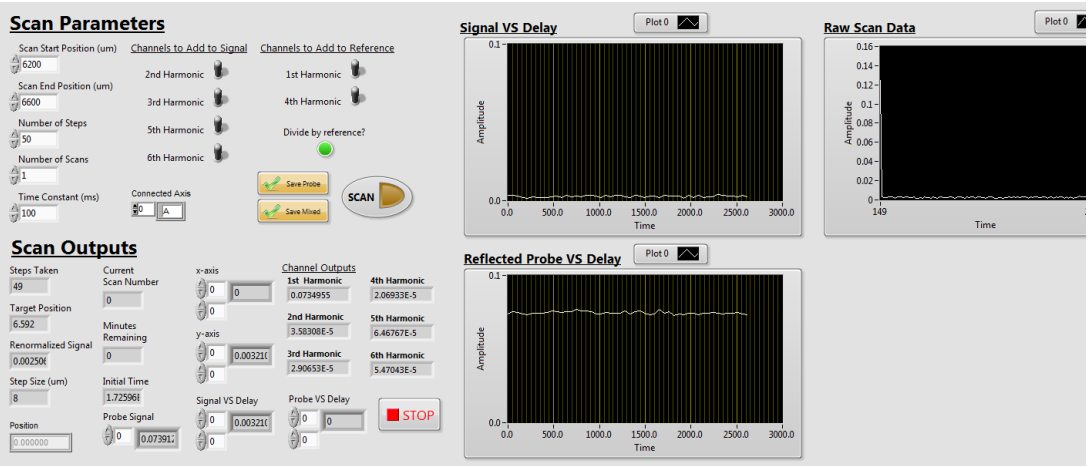

Figure 16 Screenshot of rewritten scanning program.

4.3. Thermal Excitation

As an additional supplement to the pump-probe spectroscopy, I wanted to observe the thermal excitation of my samples. Though the pump-probe system was designed to measure the optical excitation of materials, we developed a temporary modification in order to drive the transition with heat as well. For the sake of maintaining the current functionality of the system, this modification had to leave the vast majority of the system untouched and be easily removed, if necessary.

The basis of the modification was the desire to both control and monitor the temperature of the data while still being able to measure the reflectivity (the best indication of the transition). The comfort in designing the modification was that this measurement had no need for time resolution, as the transition would be purely dependent on temperature. This meant I didn't have to worry about any programming on the delay stage at all; we only wanted one small beam.

The solution was to use only half of the original system. As we didn't want to drive the transition optically, we only wanted to use the probe beam. In order to do this, we simply placed

a beam block in front of the pump arm after the beamsplitter. This left the probe free to go to the sample but prevented any influence the pump might have on the state of the material. I would then be able to monitor the signal of the probe on the lock-in amplifier, using the probe's frequency channel (rather than the mixed frequency channel this time).

In order to control and monitor the temperature, I was able to borrow a system that had been designed for a previous experiment. This consisted of a small heating stage with an attached thermocouple and a Proportional-Integral-Derivative (PID) controller system. The heating stage was mounted on a small stainless steel plate, which I was easily able to attach to the magnetic mount where I normally placed my samples. I was then able to run the attached thermocouple and coaxial cables across the table and down to the location of the controller system. I then had to readjust the mount holding the heating stage to, once again, be at the focus of the probe beam.

The controller system works by taking a reading on the temperature of the heating stage via the thermocouple. Based upon the difference between that temperature and the set temperature of the system, the controller then sends a signal to the power supply which puts out a voltage accordingly to either bring the system's temperature up or down. This process continuously reiterates, ensuring that the system remains at the temperature set by the user.

In order to get a graph of signal versus the temperature, I would set the PID to a certain value and wait for the temperature to come to an equilibrium. I would then take note of both the temperature and the signal reading on the lock-in amplifier software and move to the next point. I continued to repeat this procedure until the scan was complete.

5. RESULTS AND ANALYSIS

I studied two particular samples of VO_2: a polycrystalline film and a single crystal rod. Visuals of both of these samples are shown in Fig. 17.

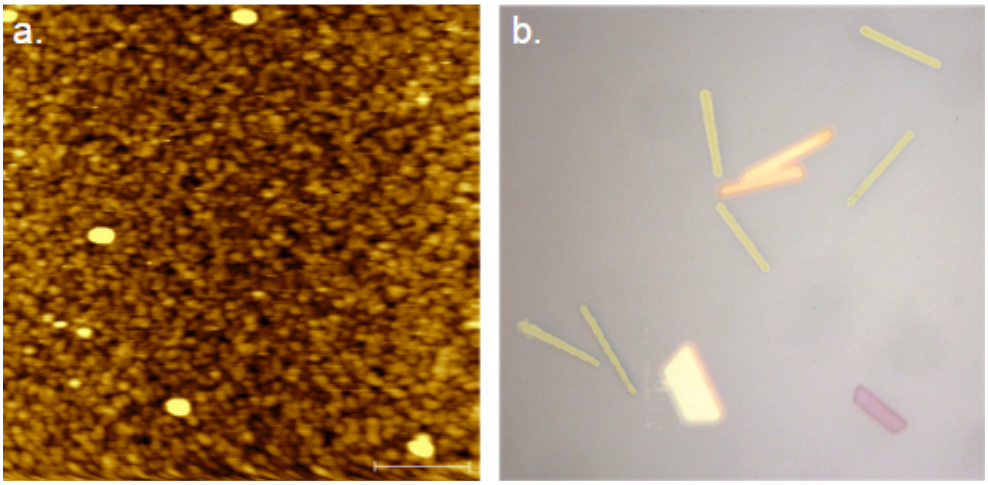

Figure 17 (a) Topography of polycrystalline sample of vanadium dioxide. (b) Picture of single crystal rod sample showing variation between individual rods.

Notice that the entire surface of the polycrystalline sample is covered in VO_2, while the rods in the single crystal sample make up only a small portion of the surface area. Due to this, aligning the system for the measurement of the polycrystalline sample was simpler than doing the same for the other. On a secondary note, the varying colors of the rods make little difference in the scan, though they are an important reminder of the inhomogeneity of just a single sample.

5.1. Fluence Dependence

I began by looking at the single crystal VO_2 sample. By adjusting the attenuator, I was able to vary the fluence and observe the sample at various levels of stimulation. The results are shown in Fig. 18.

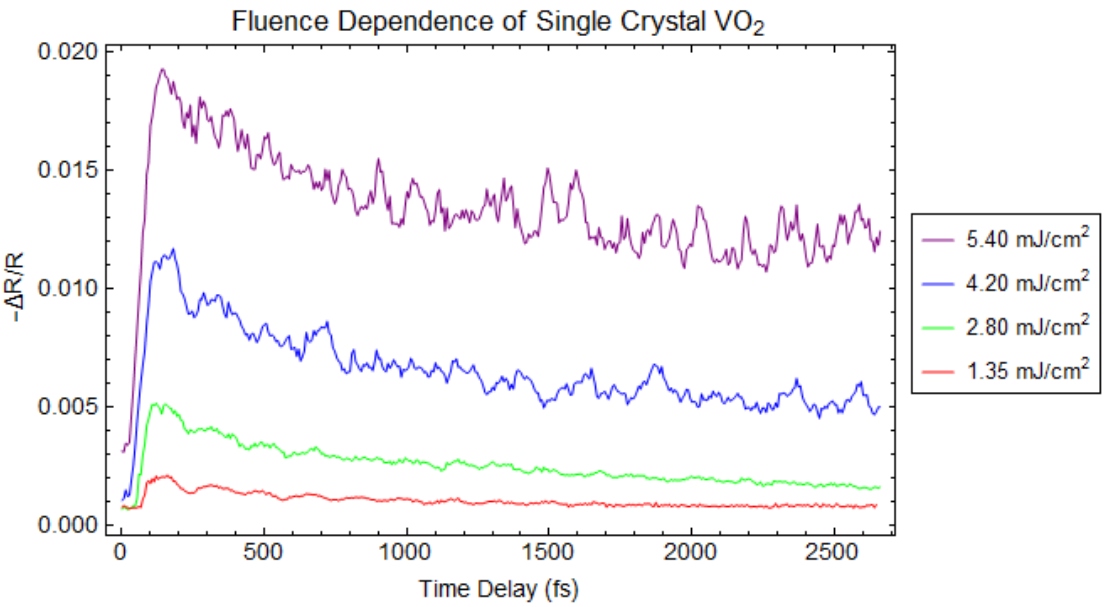

Figure 18 The fluence dependence of single crystal VO_2.

The highest fluence levels I used produced a response similar to the initial test we ran. This is very close to a full transition, though it is important to recognize that there is certainly a decay in this transitioned state. This decay is present at all of the levels of fluence shown here. However, at higher fluences, the decay is not as prevalent (as in the initial test). In this case, my colleagues advised that I avoid scanning above 6 mJ/cm^2, for the safety of the sample as any fluence above that might burn it.

I compared my data to that taken on a similar sample by another member of my group (shown in Fig. 19, below). My results were consistent with what had been previously found. My group member, however, observed a full transition at 4.3 mJ/cm^2 while I was unable to observe the same at a higher fluence. The variations observed between rods accounts for this discrepancy.

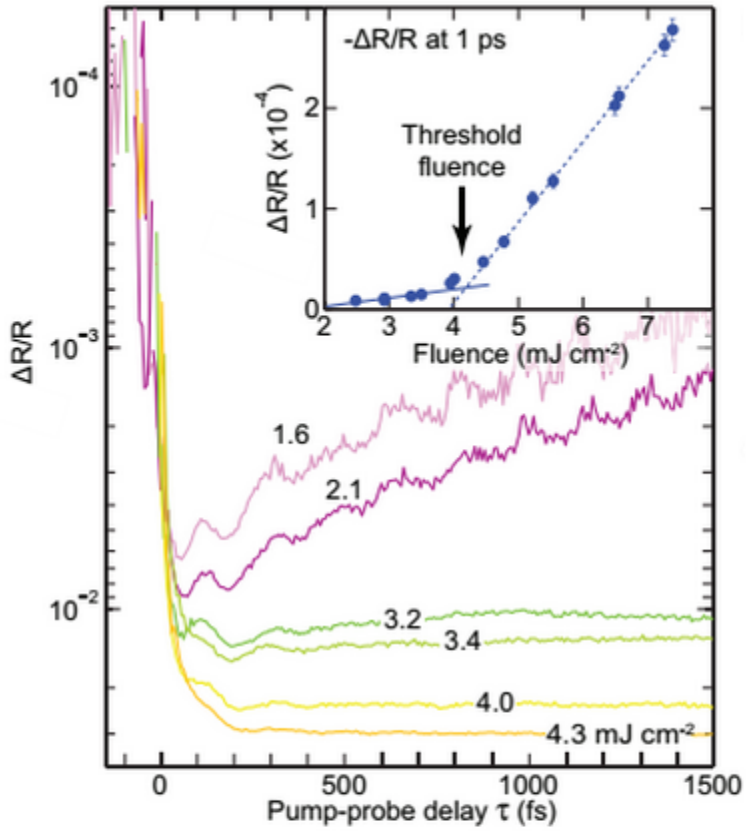

Figure 19 Fluence dependence for a particular crystal. Inset shows reflectivity VS fluence and demonstrates a change in the relation after threshold fluence. [7]

5.2. Below Threshold Fluence

The most interesting development of this particular experiment was the appearance of oscillations at lower fluence levels. These are visible in the two lowest fluences levels in Fig. 18. The oscillations are, in fact, phonons propagating on the surface of the sample. A phonon is a collective excitation of particles in a material resulting from some sort of perturbation. The effect is analogous to ripples on the surface of a lake. In this case, the phonons appear when the energy transferred to the sample by the pump beam is not enough to produce a full transition. As the transition accompanies a lattice distortion, the lack of a full transition but presence of extra

energy results in vibrations in the lattice structure. These vibrations produce a variation in the reflectivity of the sample, which we can see in the probe signal during our scan. The implications of coherent phonon observation are similar to those of Raman spectroscopy. By observing the frequency of the lattice vibrations, we may be able to determine the chemical composition and structure of certain materials.

In light of this observation, we decided to take more detailed scans of the samples below threshold fluence (the fluence at which we observe a full transition). We began by taking eight consecutive scans at the same fluence level and rod position on the single crystal sample. Once we had obtained this data, I performed a fit on the exponential decay of the scans and subtracted this fit from the data, in order to observe only the coherent phonon response. This is shown in Fig. 20, below.

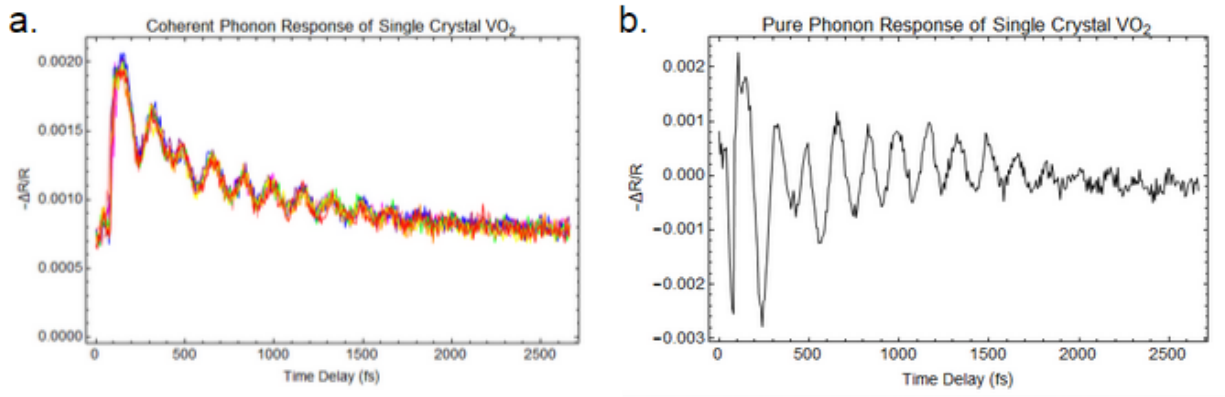

Figure 20 (a) Plotted data from 8 consecutive scans of the single crystal sample. (b) Data without the exponential decay resulting in the pure phonon response.

I repeated this experiment and fitting procedure with the polycrystalline sample at the same repetition rate and fluence. This time, however, I only took four scans as I believed this to

be sufficient to observe the phenomenon I wanted to capture. The results are shown in Fig. 21, below.

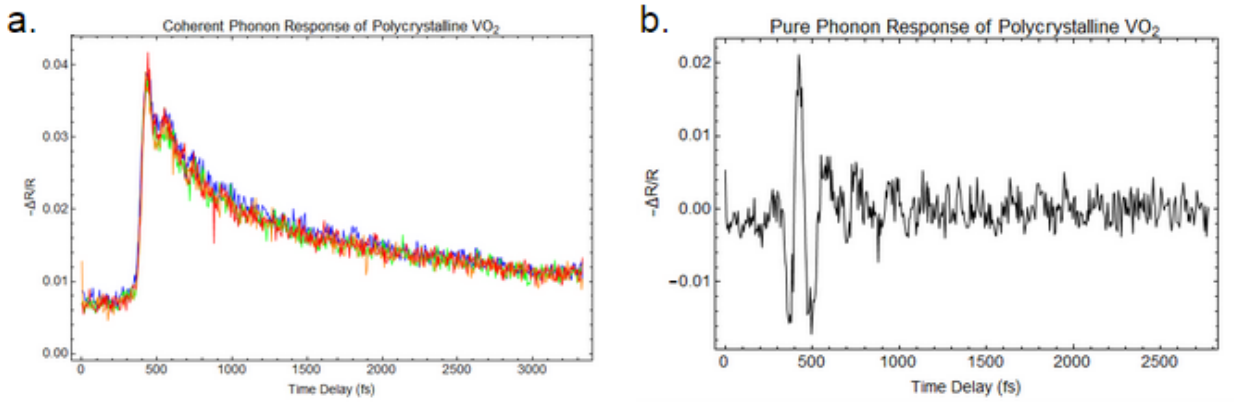

Figure 21 (a) Plotted data from 4 consecutive scans of the polycrystalline sample. (b) Data without the exponential decay.

It is immediately apparent that the phonons in the thin film were much less pronounced. The noise in the signal response makes it difficult to pick out the oscillation at a glance. Once the exponential decay was subtracted, the oscillation became a bit easier to see but they were much more damped than those observed in the single crystal sample. In order to analyze these graphs further, I took a Fourier transform of both of the revised data sets. The transforms are shown in Fig. 22.

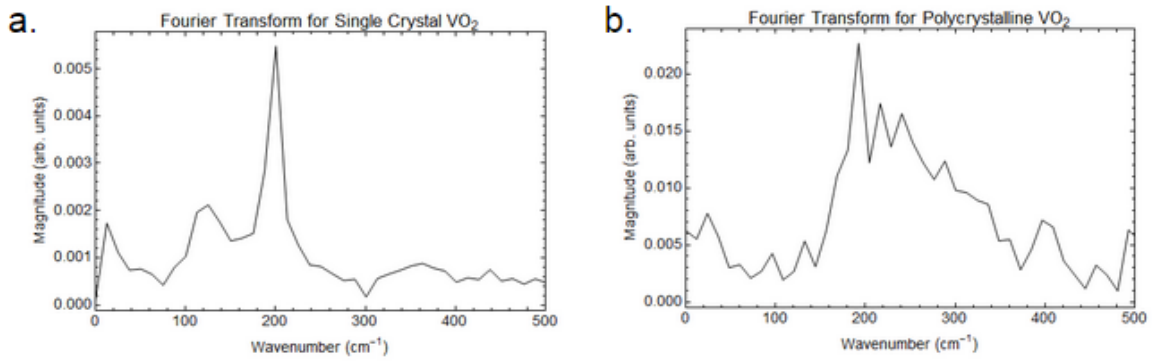

Figure 22 Fourier transform of coherent phonon response in (a) single crystal sample with highest peak at 200cm^{-1} and (b) polycrystalline sample with highest peak at 190cm^{-1}.

The largest differences between these two graphs is the linewidth of the peaks in each: the linewidth of the polycrystalline peak is, evidently, much larger than that of the single crystal. This is due to the large damping of the coherent phonons within the polycrystalline sample. A difference in the damping of these phonons between the two samples could indicate distinct structural constraints resulting from growth methods.

Additionally, though the peaks of these two transforms are in nearly the same location, the difference in their positions may also provide insight to the structure of each crystal. Recall that, within VO_2, there are three distinct insulating phases: M1, M2, and T. Each of these phases corresponds to a different level of tensile strain in the sample which results in changes in the values of the precise phonon frequencies [15]. From this observation, it is possible that the differences in phonon frequencies between these two samples are due to differences in strain. At $190cm^{-1}$, we would expect the polycrystalline sample to be experiencing less tensile strain than the single crystal sample, at $200cm^{-1}$.

It must be noted that this secondary inference is, by no means, conclusive. It is meant to be, much more so than a conviction, an exploratory gesture at another potential underlying factor. In addition to the low spectral resolution in these graphs, the comparison between the response of phonons in a single crystal sample to those in a polycrystalline sample has no precedent. It may, however, indicate another difference resulting from the methods of growing these two samples. This possibility may be worth exploring further.

5.3. Above Threshold Fluence

For the sake of comparison, I decided to look at the above threshold fluence behavior as well. I took one scan for each sample of the full transition to the metallic state at a fluence above the threshold. Though the fluence thresholds for these two samples were not the same, as long as I scanned above the threshold, very little changed. The two scans are shown in Fig. 23.

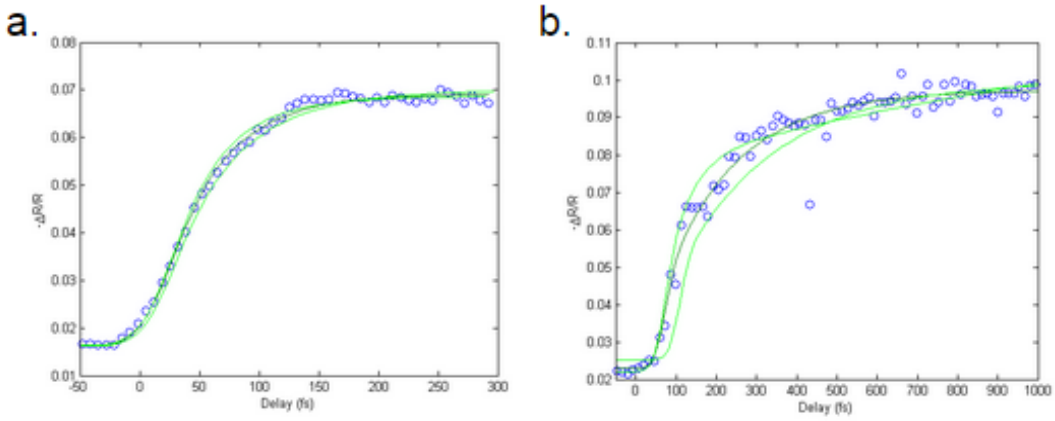

Figure 23 Above threshold fluence in (a) single crystal and (b) polycrystalline VO_2.

The two transitions look very similar. As they were taken at different fluences, a comparison of just the magnitudes would not mean much. There is, however, one particular variable to take notice of. The time duration of the transition seems to be different for the two samples. Examining the data in Fig. 23, the transition in the single crystal sample appeared to happen on a shorter timescale than in the polycrystalline sample.

In order to get a better grasp of the difference, we fit this data to a double exponential recovery function convoluted with the pulse duration. The single crystal sample had a fitted transition time of 47 ± 8 fs while the polycrystalline had 180 ± 90 fs. The amount of noise in the polycrystalline scan prevented us from getting a very solid value for the transition time, but the fit still looks pretty good.

The result for the single crystal sample falls within the range described by recent literature (40 fs - 200 fs transition) [7]. However, it disagrees with older literature, which made claims that the transition must be longer than 75 fs, as limited by a structural bottleneck [4]. These contradictory results suggest that the transition is not limited by structural timescales set by phonon frequencies.

The main difference between these two samples is the long term behavior. In the single crystal sample, the full transition is very quickly achieved and we observe very little long scale increase. In the polycrystalline sample, however, the transition is much longer and the data indicates a steady increase in the reflectivity at longer time scales. This may indicate long term thermal effects on the thin film which are not present in the rod: an observation which would agree with the inhomogeneity previously observed in thin film samples [7]. These thermal effects are due to the manner in which the sample is studied. In the single crystal sample, the pump beam entirely covers only one crystal. As such, the transition is induced in only that crystal.. In the polycrystalline sample, however, the pump beam covers multiple crystals. Due to inhomogeneity within the sample, each of these crystals has a difference threshold fluence. Therefore, in the few femtoseconds after the pump hits, only a handful of these crystals transition. As time goes on, however, heat begins to move through the sample, inducing a transition in neighboring crystals. The result is a decrease in reflectivity over longer timescales due to this rolling transition. Again, this result is not yet conclusive, but may validate further research in this area.

5.4. Additional Data

As a complement to what I had already observed, I also looked at the thermally induced transition, rather than just the optical. For this experiment, I only looked at the polycrystalline sample as I found it very difficult to get a signal from a rod. This difficulty may have come from not being centered enough on the sample or, perhaps, from uneven heating distribution from my thermal apparatus. In light of this, I decided to use only the thin film, which did produce a noticeable transition. Using the method described previously, I took a single scan of the sample and obtained the results shown in Fig. 24.

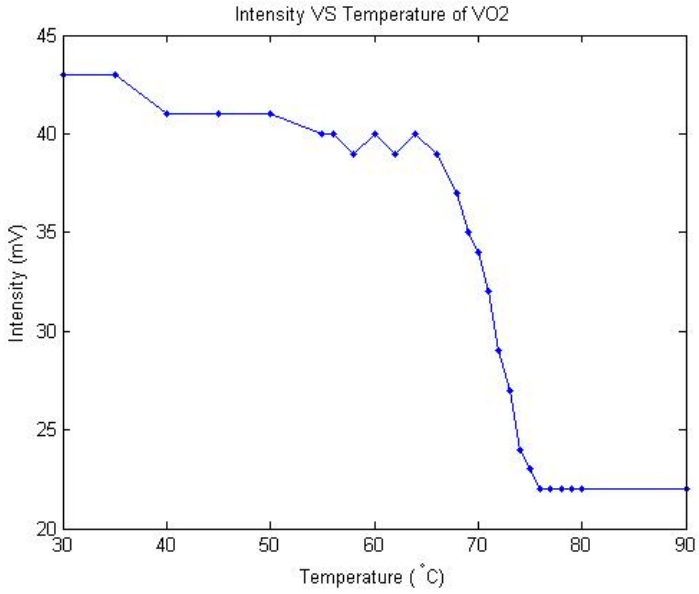

Figure 24 Thermally induced transition in polycrystalline sample.

Notice that the transition occurs at approximately 340K, which agrees with previous literature [20]. This, though not terribly enlightening, does provide further verification to the other data I have taken.

6. CONCLUSIONS AND FUTURE WORK

Throughout the course of this project, I have managed to observe a fair range of responses in two samples of vanadium dioxide. The fluence dependence behaved as expected in the single crystal sample, demonstrating an increasing dampening of the coherent phonons with increasing fluence. The thermally induced excitation in the thin film sample also behaved as predicted by literature. These two experiments helped to confirm the integrity of the samples I tested.

I was also able to observe differences in the coherent phonons induced on the surface of both samples. The discrepancy in the peak location of each of these Fourier transforms implies a potentially different induced structural distortion in each of the transitions. This, if studied more in depth, may allow comparisons of different coherent phonon behavior (frequency, damping, etc.) due to different strain states of VO_2 and its associated structural changes.

The difference in the transition time between the two samples also indicates a significant discrepancy in their respective transitions. The more prevalent long term behavior in polycrystalline sample suggests more influential thermal effects in that sample. This could also prove to be very enlightening, if studied further.

In addition to my observations, I was able to simplify the scanning program used for the pump-probe system which may allow further experimentation to be more streamlined and easy to troubleshoot. The verification of the functionality of the thermal apparatus may also prove valuable in future endeavours.

Unfortunately, I was not able to complete all of the tests I had in mind when I began. In the future, I would like to look at the fluence dependence of the thin film sample, in order to

compare it to that of the rod sample. I would also like to look at the thermally induced transition in the rod sample using this system in order to compare it to that observed in the polycrystalline. As a further test, I may also look at the repetition rate dependence in both of the samples. The differences (if observed) in these experiments may shed further light on the discrepancies between the responses in each sample and allow us to begin understanding the primary driving force which causes them.

It should also be noted that the thermal scan I took demonstrated that the method I used needs some improvement. The signal at higher temperatures fluctuated significantly and made it difficult to take an accurate measurement by only observing the lock-in software. In order to remedy this, I would like to write a new program to capture the signal from the lock-in over a certain period of time and average it, rather than using my rough approximations.

If time permits, I would also like to look at other samples, specifically calcium ruthenate and lanthanum manganate, which are both expected to undergo a metal-insulator transition. By looking at these two samples and comparing them to my observations of vanadium dioxide, I may be able to further my understanding of how they behave.

7. REFERENCES

[1] "Metal-insulator transition in vanadium dioxide,"A. Zylbersztejn and N. F. Mott, *Physical Review B* **11** 4383-4395 (1975).

[2] "Coherent Structural Dynamics and Electronic Correlations during an Ultrafast Insulator-to-Metal Phase Transition in VO_2" C. Ku bler, H. Ehrke, R. Huber, R. Lopez, A. Halabica, R. F. Haglund, Jr., and A. Leitenstorfer, *Physical Review Letters* **99** 116401 (2007).

[3] "Tracking the evolution of the electronic and structural properties of VO_2 during the ultrafast photoinduced insulator-metal transition," S. Wall, L. Foglia, D. Wegkamp, K. Appavoo, J. Nag, R. F. Haglund, Jr., J. St ähler, and M. Wolf, *Physical Review B* **87** 115126 (2013).

[4] "Evidence for a structurally-driven insulator-to-metal transition in VO_2: A view from the ultrafast timescale," A. Cavalleri, Th. Dekorsy, H. H. W. Chong, J. C. Kieffer, and R. W. Schoenlein, *Physical Review B* **70** 161102 (2004).

[5] "Monoclinic and Correlated Metal Phase in VO_2 as Evidence of the Mott Transition: Coherent Phonon Analysis," H. Kim, Y. W. Lee, B. Kim, B. Chae, S. J. Yun, K. Kang, K. Han, K. Yee, and Y. Lim, *Physical Review Letters* **97** 266401 (2006).

[6] "Orbital-Assisted Metal-Insulator Transition in VO_2," M. W. Haverkort, Z. Hu, A. Tanaka, W. Reichelt, S. V. Streltsov, M. A. Korotin, V. I. Anisimov, H. H. Hsieh, H.-J. Lin, C. T. Chen, D. I. Khomskii, and L. H. Tjeng. *Physical Review Letters* **95** 196404 (2005).

[7] “Inhomogeneity in the ultrafast insulator-to-metal transition dynamics of VO_2,” B. T. O’Callahan, J. M. Atkin, A. C. Jones, J. H. Park, D. Cobden, and M. B. Raschke. *Nat. Comm.* (2015).

[8] “Strongly Correlated Electron Materials: Insights from Dynamic Mean-Field Theory,” G. Kotliar and D. Vollhardt. *Physics Today* 53-59 (2004).

[9] “Complexity in Strongly Correlated Electronic Systems” E. Dagotto. *Science* **309** 257 (2005).

[10] “Strongly Correlated Electron Materials: Dynamical Mean-Field Theory and Electronic Structure” A. Georges. *American Institute of Physics Conference Proceedings* **715** 2-70 (2004).

[11] C. Kittel, Introduction to Solid State Physics, (Wiley & Sons, New York, 1966).

[12] B. K. Ridley, Quantum Processes in Semiconductors, 3rd ed., (Clarendon Press, Oxford, 1993).

[13] R.H. Bube, Electrons in Solids, 3rd ed., (Academic Press, Boston, 1992).

[14] “Electron Correlations in Narrow Energy Bands,” J. Hubbard. *Proceedings of the Royal Society of London. Series A, Mathematical and Physical Sciences* **276** 1365 (1963).

[15] “Strain and temperature dependence of the insulating phases of VO_2 near the metal-insulator transition,” J. M. Atkin, S. Berweger, E. K. Chavez, and M. B. Raschke, *Physical Review B* **85** 020101 (2012).

[16] “Nano-optical Investigations of the Metal-Insulator Phase Behavior of Individual VO_2 Microcrystals,” A. C. Jones, S. Berweger, J. Wei, D. Cobden, and M. B. Raschke. *American Chemical Society - Nano Letters* **10** 1574-1581 (2010).

[17] “Quantum Electronics”, H. Haus, J. Fujimoto, and E. Ippen. *IEEE Journal* **28** 2086 (1992).

[18] H. Mocker and R. Collins. *Applied Physics Letters* **7** 270 (1965).

[19] "Measuring Ultrashort Laser Pulses in the Time-Frequency Domain Using Frequency-Resolved Optical Gating," R. Trebino, K. W. DeLong, D. N. Fittinghoff, J. N. Sweetser, M. A. Krumbügel, and D. J. Kane. *Review of Scientific Instruments* **68** 3277-3295 (1997).

[20] “Oxides which show a metal-to-insulator transition at the Neel temperature,” Morin, F. J. *Phys. Rev. Lett.* **3** 34–36 (1959).